Journal of Food Engineering 358 (2023) 111673

Contents lists available at ScienceDirect

Journal of Food Engineering

journal homepage: www.elsevier.com/locate/jfoodeng

Study of light penetration depth of a Vis-NIR hyperspectral imaging system for the assessment of fruit quality. A case study in persimmon fruit

Alejandro Rodríguez-Ortega [a], Nuria Aleixos [a], José Blasco [b], Francisco Albert [a], Sandra Munera [a,*]

[a] Departamento de Ingeniería Gráfica, Universitat Politècnica de València, Camino de Vera, S/n, 46022 Valencia, Spain
[b] Centro de Agroingeniería, Instituto Valenciano de Investigaciones Agrarias (IVIA), Carretera CV-315, Km 10.7, 46113, Moncada, Spain

ARTICLE INFO

Keywords:
Light depth penetrability
Fruit
Scattering
Absorption
Optical properties
Hyperspectral imaging

ABSTRACT

Hyperspectral imaging (HSI) is one of the most studied optical techniques to estimate the internal quality of fruits and vegetables. Absorbance and reflectance of the light radiation are specific to each biological tissue and are directly related to its chemical composition and physical characteristics. These properties are influenced by other extrinsic factors, such as the instrumentation or the light source, which can reduce the reproducibility of the experiments. Determining the actual depth of light penetration into tissue could help validate non-contact methods as accurate tools to assess quality properties based on optical properties. In the case of HSI systems, it is crucial to know how far the light penetrates at each wavelength. A non-destructive approach, based on the spatially resolved spectroscopic principle, was proposed to estimate the light penetration depth of a HSI system in a Vis-NIR configuration (in the range 450–1050 nm). This method was applied to measure the light penetration depth in persimmon fruit. The absorption (μ_a) and scattering (μ'_s) coefficients from Farrell's diffusion theory were estimated using the backscattered light measured at different distances from the incident point light at each wavelength in hyperspectral images of persimmon fruit. The actual light penetration depth was obtained by measuring the reflectance of cut pieces of persimmon fruit with different thicknesses. Linear regression was used to relate the depth of penetrability obtained by both protocols, the estimated or non-destructive protocol and the actual or destructive protocol, showing a high relationship ($R^2 > 0.8$ and RPD>2.5) in the range 610–1050 nm. This confirms that this non-destructive approach proposed for estimating the light penetration depth of a Vis-NIR HSI system in persimmon fruit is accurate, so it could be used as a valuable method to evaluate other HSI systems for different fruits.

1. Introduction

HSI is an effective technique for assessing the internal quality of fruits and vegetables (Hemrattrakun et al., 2021; Munera et al., 2021; Xuan et al., 2022). The HSI systems capture a sequence of monochromatic images in a spectral operating range, the most used operating in the Vis and NIR spectral ranges. When a biological tissue is illuminated, the chemical compounds absorb or reflect the energy differently for each wavelength, allowing HSI systems to get information on the intrinsic properties and chemical composition non-destructively (Rodrigues and Hemmer, 2022). HSI systems are characterised by obtaining spatial and spectral information so that a full spectrum is obtained for each pixel acquired, which allows knowing the composition of the tissues and how the properties are distributed on the surface. It makes it especially useful for inspecting heterogeneous products such as fruits or vegetables.

The propagation of light through biological tissues is influenced by various optical properties such as absorption, scattering, refraction, and reflection. Absorption refers to the ability of tissues to absorb certain wavelengths of light, which can limit the depth of light penetration. Refraction is related to the change in the direction of light when it enters a medium with a different refractive index, such as air and biological tissues. Refraction can affect the propagation of light through tissues, especially in cases where the tissues have a curved surface. Finally, reflection refers to the ability of tissues to reflect light rather than allow it to pass through. The amount of light that is reflected depends on the angle of incidence of the light according to Lambert's cosine law (Pedrotti et al., 2007), as well as on the optical properties of the tissues. Finally, scattering is the ability of tissues to deflect light from its original

* Corresponding author.
E-mail address: sanmupi@upv.es (S. Munera).

https://doi.org/10.1016/j.jfoodeng.2023.111673
Received 16 June 2023; Received in revised form 25 July 2023; Accepted 28 July 2023
Available online 29 July 2023

Nomenclature

CCD	charge couple device
FR	frequency domain
HSI	hyperspectral imaging
NIR	near infrared region
RH	relative humidity
RMSE	the root mean square error
ROI	region of interest
RPD	ratio of performance to deviation
R^2	coefficient of determination
SFD	spatial frequency domain
SR	spatially resolved
TR	time-resolved
Vis	visible
μ_a	absorption coefficient
μ'_s	scattering coefficient

path. This can occur due to variations in the refractive index or the presence of particles in the composition of tissues that can bend light. Fruit have particular characteristics that can affect the penetration and propagation of light inside them depending on the texture and composition (Sun et al., 2021). For example, the skin of a fruit can limit the amount of light that penetrates into the fruit. Moreover, the presence of pigments that absorb certain wavelengths can influence the characteristics of the light that penetrates into the fruit tissue (Saeys et al., 2008), while the texture, the water content and chemical composition can also affect the diffusion of light, and therefore its ability to absorb, reflect, scatter, or refract light (Hu et al., 2015; Munera et al., 2017, 2019). Moreover, extrinsic factors, such as the instrumentation or the light source, influence how the light interacts with the tissues, reducing reproducibility (Lu et al., 2020).

Absorption and scattering phenomena characterise light propagation through the tissue, which can provide information about the internal composition of the samples under study (Cen et al., 2012a,b; Sun et al., 2021; Vanoli et al., 2020). These optical properties can be usually quantified by the μ_a, which is the probability of a photon being absorbed by pigments or chemical constituents in the tissue (Vanoli et al., 2020), and the μ'_s, which is the probability of a photon changing direction due to refractive index mismatches in the tissue microstructures (Vanoli et al., 2020, Ying et al., 2016), and is affected by the physical properties of the tissue, such as texture, cell density or cell volume (Ma et al., 2022). However, fruit tissues are highly scattering media (Wang et al., 2020), so separating the scattering effects from light absorption is difficult.

Backscattering refers to the scattering of light in the opposite direction to its incidence, that is when the light scatters back near the source (Lorente et al., 2015). The backscattered light interacts with the more superficial tissue and exits close to the incidence light point, containing information about the texture or composition that can be assessed, for instance, using a HSI system. It is uncertain, though, how deeply the light penetrates the fruit before exiting, making it unclear from which internal part this information originates, as this issue is hardly discussed in the literature (Lorente et al., 2013). Therefore, it is necessary to explore new approaches to understand and measure the behaviour of the backscattered light, considering different wavelengths independently of any external factors, to achieve more reproducible and reliable experiments.

Non-destructive methods are available to separately measure the absorption and the reduced scattering coefficients of biological tissues. These methods are based on analytical solutions to the diffusion approximation theory in different lighting conditions and can be classified into SR, TR, FR and SFD (Tian and Xu, 2022). The SR method estimates the absorption and reduced scattering coefficients by measuring the reemitted light at different distances from a steady-state light, illuminating a small area of the biological sample (Kienle et al., 1996). The TR method uses ultrashort laser pulses, which are fallen upon the sample surface. Then, the coefficients are estimated by processing the temporal response of the reemitted light acquired at a proximity distance to the point of incidence of light (Wilson et al., 1989). The concept of the FR technique is similar to TR. In this method, a high-frequency modulated light signal falls on the tissue, and its output at a specific distance from the incidence area is then analysed to estimate the coefficients (Berndt et al., 1991). Finally, the SFD method uses different 2-D sinusoidal illumination patterns to light the sample under study to acquire and process the reflectance images to estimate the coefficients for these optical properties (Hu et al., 2018). SR methods are the best suited for fruit postharvest studies since they do not require expensive instrumentation nor good contact between the sensor and the fruit tissue, are faster than TR and FD ones, and are easier to implement in an automated inspection set-up (Qin and Lu, 2008).

Two typical configurations of SR techniques differ in whether their sensing is by contact or non-contact with the sample. In the first case, an optical fibre array is used to acquire the reemitted light at various points in the tissue, located at different distances from the incident light point. By contrast, HSI is non-contact sensing used in SR techniques, and it can be used to evaluate the absorption and reduced scattering at multiple wavelengths by diffuse scattering or backscattering imaging, providing spatial and spectral information for a broad spectral range (Si et al., 2022). Its configuration requires mainly a CCD camera, an imaging spectrometer, and a light source, concentrating a small continuous-wave light beam on the sample surface (Cen et al., 2012a,b). Then, backscattered light, measured at different distances from the incident light at each wavelength, is fitted to obtain the absorption and reduced scattering coefficients related to the optical properties of the tissues (Van Beers et al., 2015; Zhu et al., 2015). However, these coefficients measured by SR techniques only provide an estimation of the actual absorption and scattering of the tissue under study. Therefore, it becomes necessary to know both the actual values of these parameters and the depth at which they are measured to establish the reliability of the HSI-based systems in estimating the absorption and scattering of fruit tissues.

Qin and Lu (2008) defined the light penetration depth as the distance travelled by the light within a biological tissue until the incident light intensity level is reduced by 1/e. Light penetration depth is related to the attenuation of light in vegetables and fruits, and as a consequence, it involves both absorption and scattering properties. Therefore, estimating the light penetration depth could be helpful to validate the estimated absorption and scattering properties of a tissue obtained by HSI systems (Kho et al., 2019). validated the use of hyperspectral imaging as a tool to assess breast tissue at different depths below the resection surface. To do this, they used a phantom that simulated the spectral properties of breast tissue and thus determined the depth to which light penetrated. In our case, a similar validation could be used to measure the actual depth to which light penetrates into fruit. In this case, the phantom would be replaced by a destructive study of the fruit to determine the specific depth of the internal fruit tissue at which the optical properties are estimated.

The purpose of this work is to propose a method to estimate non-destructively the depth of light penetration of a Vis-NIR HSI system (450–1050 nm) in the tissues of the fruit. The whole study was developed on 'Rojo Brillante' persimmon fruit, and proceeded as follows: (1) the absorbance and scattering were non-destructively estimated by applying the Farrell's diffusion theory using backscattering images of the entire fruit; (2) the actual light penetration depth was subsequently measured by means of an ad-hoc destructive protocol using reflectance images of the entire fruit and pieces of different thicknesses; (3) As a final step, a validation of the estimated light penetration depth of each wavelength was performed by comparing it with the actual light

penetration depth by means of linear regression.

2. Materials and methods

2.1. Estimation of light penetration depth. Farrell's diffusion theory

Light backscattering in fruit occurs when light enters a fruit, interacts with cells, tissues, and other structures, and is scattered back out near the point of incidence. The amount of backscattered light from a fruit can provide valuable information about its quality, ripeness, and other properties (Lu et al., 2020b). This phenomenon can be modelled on the radiative transfer theory (or the Boltzmann equation), which can be simplified to a diffusion approximation equation for highly scattering biological tissue, i.e., $\mu'_s \gg \mu_a$ (Cen et al., 2012a,b; Lu et al., 2017; Qin and Lu, 2008). Therefore, the Boltzmann equation can be simplified to only two independent optical parameters, μ_a and μ_s, and can be resolved analytically by the information acquired through various techniques based on different illumination situations (Lu et al., 2020).

SR measurement system can resolve this equation by measuring the backscattered light at different distances from a steady-state incident light source (Hu et al., 2015), as shown in Fig. 1, fitting the reflectance curve to the Farrell's diffusion equation (Eq. (1)) (Farrell et al., 1992).

$$R(r) = \frac{C_1}{4\pi D}\left[\frac{e^{-(\mu_{eff} r_1)}}{r_1} - \frac{e^{-(\mu_{eff} r_2)}}{r_2}\right] + \frac{C_2}{4\pi}\left[\frac{1}{\mu'_t}\left(\mu_{eff} + \frac{1}{r_1}\right)\frac{e^{-(\mu_{eff} r_1)}}{r_1^2} + \left(\frac{1}{\mu'_t} + 2z_b\right)\left(\mu_{eff} + \frac{1}{r_2}\right)\frac{e^{-(\mu_{eff} r_2)}}{r_2^2}\right] \quad (1)$$

where r is the distance from the incident light point, D is the diffusion coefficient (Eq. (2)), μ_{eff} is the effective attenuation coefficient (Eq. (3)), μ'_t is the total attenuation coefficient (Eq. (4)), and r_1 (Eq. (5)) and r_2 (Eq. (6)) are the distances from the observation point at the interface to the isotropic source and the image source z_d (Eq. (7)) (Hu et al., 2015). R_{eff} is the effective reflection coefficient (Eq. (8)). A standard refractive index for horticultural products is $n = 1.35$, where C_1 and C_2 are 0.1277 and 0.3269, respectively (Cen et al., 2012a,b). Finally, d_{th} is the light penetration depth (Eq. (9)) and is defined as the distance at which the light fluence rate is reduced by a factor of $1/e$ of its value at the surface (Kho et al., 2019; Wilson and Jacques, 1990).

$$D = \frac{1}{3(\mu_a + \mu'_s)} \quad (2)$$

$$\mu_{eff} = \sqrt{3\mu_a(\mu_a + \mu'_s)} \quad (3)$$

$$\mu'_t = \mu_a + \mu'_s \quad (4)$$

$$r_1 = \left[\left(\frac{1}{\mu_a + \mu'_s}\right)^2 + r^2\right] \quad (5)$$

$$r_2 = \sqrt{\left[\left(\frac{1}{\mu_a + \mu'_s} + 2z_b\right)^2 + r^2\right]} \quad (6)$$

$$z_b = \frac{2(1 + R_{eff})}{3(\mu_a + \mu'_s)(1 - R_{eff})} \quad (7)$$

$$R_{eff} = 0.636n + 0.668 + \frac{0.71}{n} - \frac{1.44}{n^2} \quad (8)$$

$$d_{th} = \frac{1}{\sqrt{3\mu_a(\mu_a + \mu'_s)}} \quad (9)$$

2.2. Fruit samples

Sixty persimmon fruits (*Diospyros kaki* cv 'Rojo Brillante') were collected from a commercial orchard located in L'Alcudia (Valencia, Spain) at commercial maturity. The fruits were selected with homogeneous colour and size (weight [mean ± std]: 273.78 ± 45.11 gr; height: 82.05 ± 4.00 mm; width: 74.62 ± 5.69 mm) and no skin damage. Throughout the experiment, the fruits were stored in stable conditions (20 °C and 90% RH).

'Rojo Brillante' persimmon is an astringent cultivar due to water-soluble tannins present in the flesh. For this reason, this cultivar is usually exposed to a CO_2 treatment in a closed container (air containing 95%, CO_2 at 20 °C and 90% RH) for 24 h to remove the astringency before commercialisation (Salvador et al., 2007). During the treatment, the water-soluble tannins with low molecular weight are converted into high molecular weight, water-insoluble, and non-astringent tannins (Das et al., 2020; Giordani et al., 2011). The molecular weight of tannins changes during the deastringency treatment, and so do the optical properties, which makes this fruit appropriate for this study. Hence, half of the persimmons (30 out of 60) were deastringed through the CO_2 treatment to obtain a heterogeneous set of fruit samples.

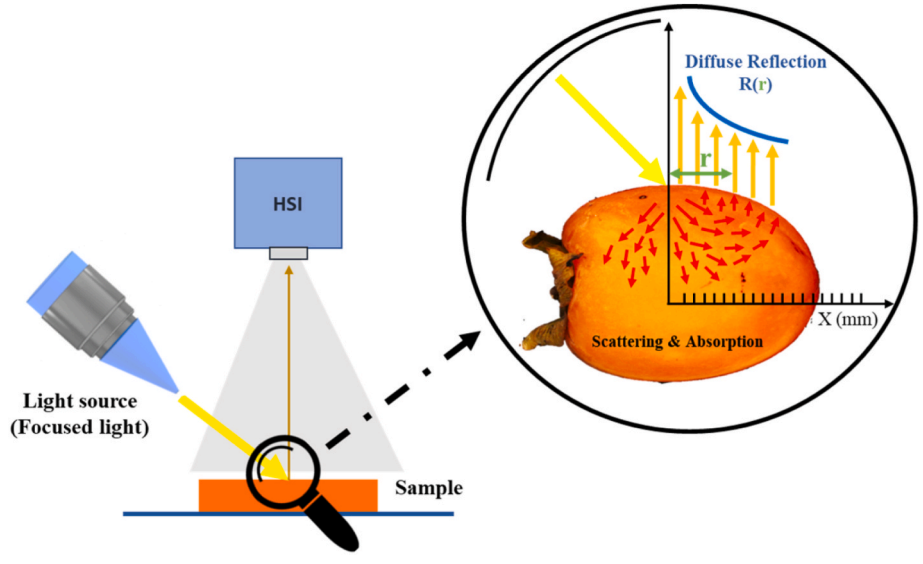

Fig. 1. HSI-based in-house bench-top prototype for the non-destructive estimation of the penetrability depth.

2.3. Hyperspectral image acquisition

2.3.1. Non-destructive protocol for penetrability estimation

Backscattering images of the entire persimmon fruit were captured with the set-up depicted in Fig. 1 using an in-house bench-top optical prototype. This HSI-based prototype was developed using the SR spectroscopic principle (Sun et al., 2021). It consisted of an industrial camera (CoolSNAP ES, Photometrics Tucson, AZ, USA) coupled with two liquid-crystal tunable filters (Varispec VIS-07 and NIR-07, Cambridge Research & Instrumentation, Inc., Hopkinton, MA, USA) (Munera et al., 2021; Munera et al., 2021), operating in the spectral range of 450–1050 nm and capturing images in reflectance mode with a size of 1392 × 1040 pixels and a spatial resolution of 0.14 mm/pixel. The integration time for each wavelength was calibrated to optimise the dynamic range of the camera, avoid saturated images, and correct the spectral sensitivity of its components. This was accomplished by acquiring the average grey level of a calibration target (Spectralon 99%, Labsphere, Inc, NH, USA) that represents 90% of the camera's dynamic range. The backscattering images were captured every 10 nm for a total of 60 wavelengths. The fruit was illuminated by direct, focused light on top of the fruit using a 35 W halogen spotlight (41,866 WFL OSRAM GmbH, Munich, Germany) powered by a direct current of 12 V. Additionally, white and black reference images were acquired using the white calibration target (Spectralon 99%, Labsphere, Inc, NH, USA) and covering the lens with the cap, respectively.

2.3.2. Destructive protocol for measuring the actual penetrability

For the validation of the previously proposed non-destructive method, the actual light penetration depth was measured following the method presented by Kho et al. (2019). Thereby, each persimmon fruit was cut into pieces (on average, sixteen pieces per fruit containing peel) of different thicknesses using a professional slice cutter (Graef Master 3020 W, Germany) and then measured using a precision digital calliper (Mitutoyo 500-182-30, Co. Ltd., Japan) resulting thicknesses between 0.3 and 19.5 mm. Later, both the fruit pieces and the entire fruit were placed onto a black background platform with the peel facing the camera, and reflectance images were acquired using the same camera as previously used but performing a new calibration of the integration time of each wavelength. In this configuration, the fruit was illuminated by diffuse light using the same halogen lamp described for backscattering images (Fig. 2).

2.4. Image processing and statistical data analysis

The image processing started with the calculation of the relative reflectance of all images through Equation (10) (Geladi et al., 1985).

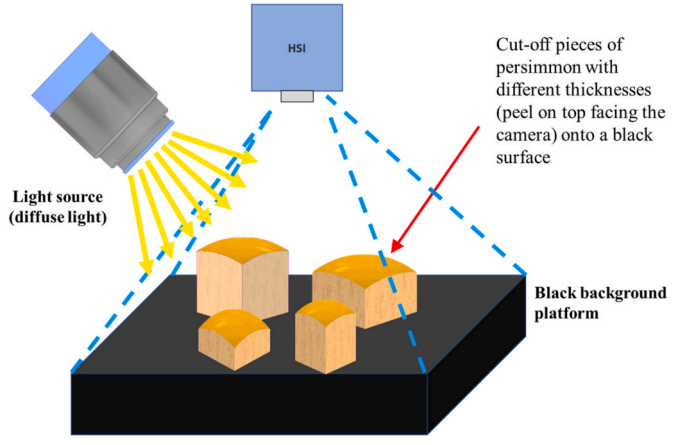

Fig. 2. HSI-based in-house bench-top prototype for the actual measurement of penetrability depth.

$$\rho_{xy}(x,y,\lambda) = \rho^{Ref}(\lambda)\frac{R(x,y,\lambda) - R_{black}(x,y,\lambda)}{R_{white}(x,y,\lambda) - R_{black}(x,y,\lambda)} \quad (10)$$

where $p^{Ref}(\lambda)$ is the standard reflectance of the white reference target (99% in this work), R (x,y,λ) is the reflectance of the fruit captured by the camera, Rwhite (x,y,λ) is the reflectance of the white reference target, and Rblack (x,y,λ) is the reflectance captured while avoiding any light source in order to quantify the electronic noise of the sensor.

Then, the central ROI of the fruit zone of all images, entire fruit and cut pieces, was selected. The reflectance of each ROI from the images of the cut pieces was then normalised by the maximum reflectance obtained from the central ROI of the entire persimmon, which will act as the infinite thick sample. No spectral pre-treatment was applied so as not to affect potentially the estimation of the light penetration depth. The reflectances were plotted against the thickness of each piece, and an exponential curve was obtained for every wavelength (Fig. 3). As stated by Welch et al. (2010), the observed exponential attenuation of reflectance is given in highly scattering tissues, where the decrease in incident diffuse light is related to the thickness of the tissue under study. Thus, the curves were fitted to Equation (11) to model the evolution of the reflectance for each wavelength concerning the thickness of the piece. Finally, the actual objective penetrability was defined as the depth required to reduce the relative reflectance by $1/e^2$ (Kho et al., 2019).

$$R_{rel}(\lambda, d) = 1 - f_1 e^{-f_2 d} \quad (11)$$

From all the captured backscattering images, a ROI was selected from the light incidence point (maximum intensity) towards the fruit contour (Fig. 4). Then, the mean intensity mono-exponential signal decay curves from each ROI were extracted for each wavelength following the pipeline shown in Fig. 4. The extracted distance-dependence curves were fitted to Equation (1) by a non-linear curve fitting based on least-squares applying the trust-region-reflective algorithm (Coleman and Li, 2006). Then, the absorption and the reduced scattering were calculated, and the estimated penetrability was obtained using Equation (9) for each wavelength.

Finally, a linear regression was applied to relate the actual depth with the estimated for each wavelength. This method obtains the best relationship by finding the best fit linear function. For the analysis of the goodness-of-fit parameter, the R^2, the RMSE and the RPD were used. Generally, a good model must have a high R^2 with a low RMSE and an RPD above 2.5 (Cortés et al., 2017). These parameters can be defined by Equations 12–14. Pearson's correlation coefficient was also calculated to assess this relationship.

$$R^2 = 1 - \frac{\sum_{i=1}^{N}(x_{ip} - x_{io})^2}{\sum_{i=1}^{N}(x_{io} - \overline{x_{io}})^2} \quad (12)$$

$$RMSE = \sum_{i=1}^{N}\frac{(x_{ip} - x_{io})^2}{N} \quad (13)$$

$$RPD = \frac{SD(x_{ip})}{RMSE} \quad (14)$$

All the algorithms were developed and implemented using Matlab R2020b (MathWorks, Natick, MA, USA) and the Imaging Processing Toolbox with custom Matlab scripts.

3. Results and discussion

The results of the actual and estimated light penetration depth in each wavelength are shown in Table 1. The actual light penetration depths ranged (mean ± standard deviation) from 0.33 ± 0.38 mm (500 nm) to 2.12 ± 0.89 mm (700 nm). The estimated light penetration depths ranged from 0.82 ± 0.46 mm (500 nm) to 2.00 ± 0.85 mm (1050

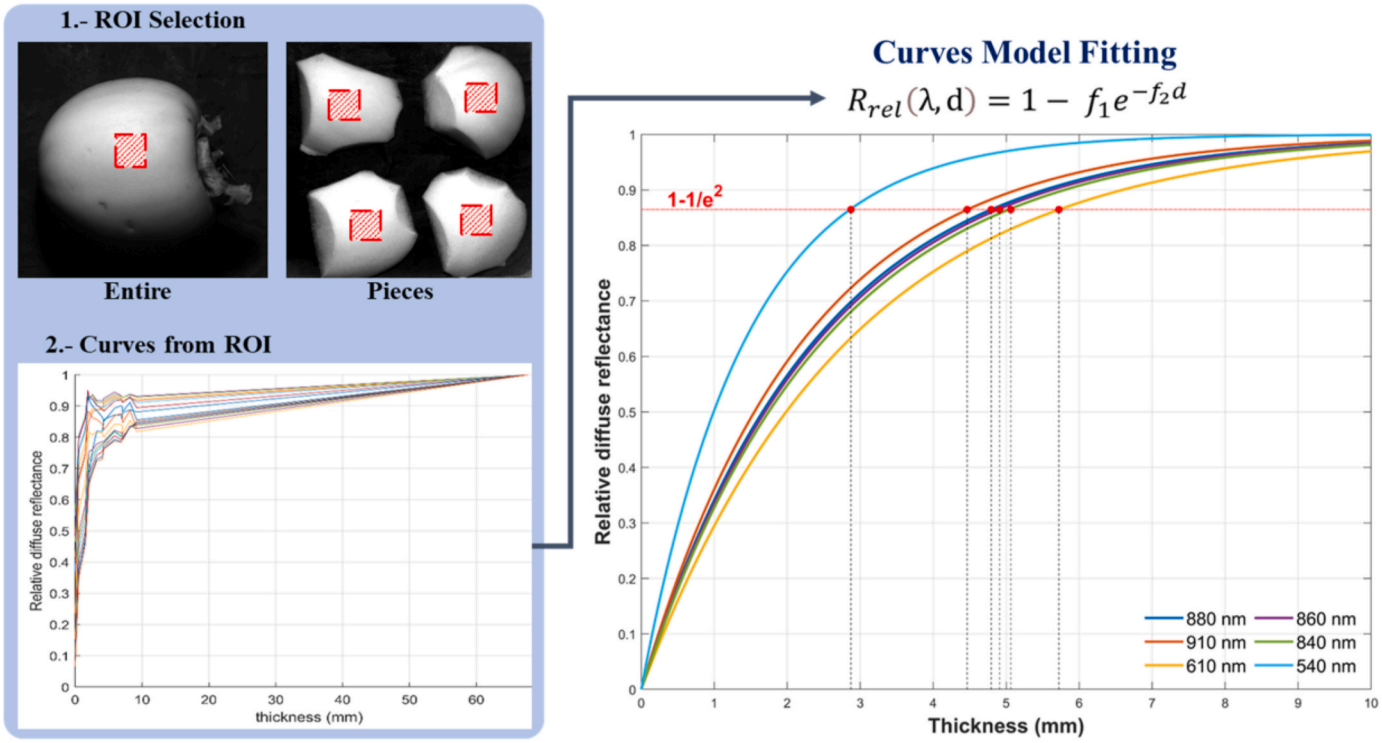

Fig. 3. Pipeline for measuring the actual light penetration depth using the set-up depicted in Fig. 2.

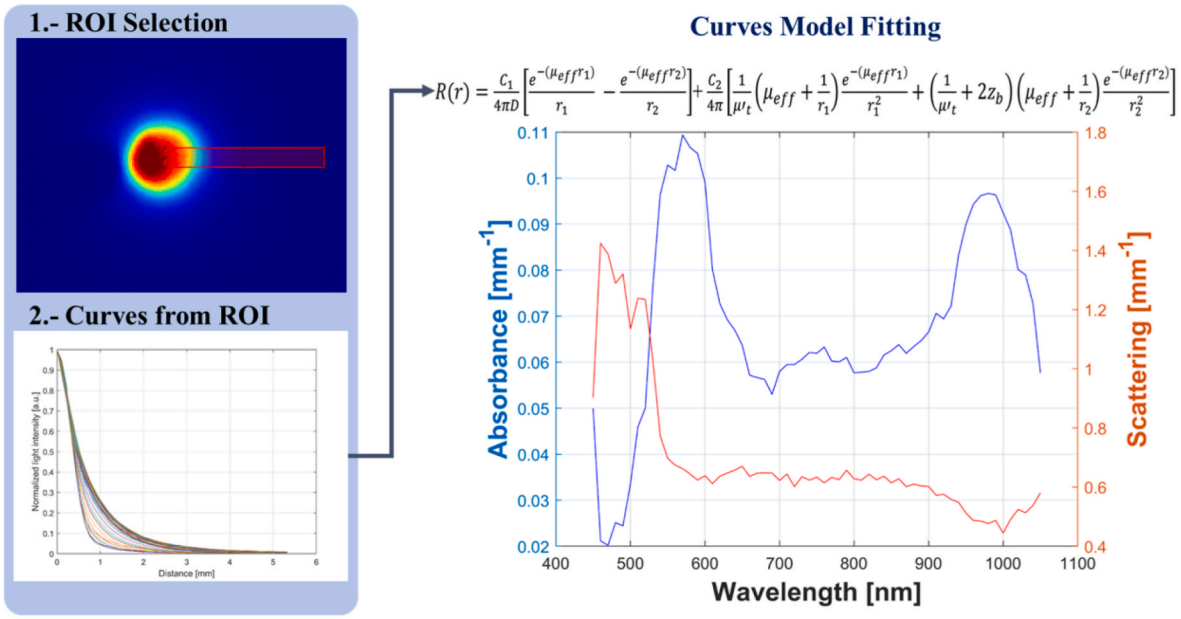

Fig. 4. Pipeline to estimate the light penetration depth using the set-up depicted in Fig. 1.

nm). These results show high variability since the selection of the samples was not carried out attending to any internal quality criteria. Furthermore, as Fig. 5 shows, no differences were found between astringent and deastringed persimmons for the averaged actual and estimated penetrability for all wavelengths.

The Pearson's correlation results (Table 1) showed a significant and positive correlation ($r > 0.92$ and p-value<0.05) for all wavelengths, except for the spectral range 510–540 nm, with high values for wavelengths greater than 610 nm. These significant correlations show a strong linear relationship between the light penetration obtained in both experiments. However, Pearson's correlation could not measure the agreement between the depth light penetration values of the non-destructive experiment and those of the destructive one.

Additionally, a linear regression was performed to compare both penetrability depths for each wavelength. A significant regression equation was found for each wavelength ($F(1,58) > 5.18$, p-value <0.02), except for the wavelengths between 510 nm and 530 nm (p-value >0.05). The estimated penetrability depth significantly predicted the actual penetrability depth (p-value <0.027) for each wavelength, except for the range mentioned above.

Table 1
Results from actual and estimated light penetration for each wavelength.

λ (nm)	Actual depth (mm)	Estimated depth (mm)	Pearson's Correlation		λ (nm)	Actual depth (mm)	Estimated depth (mm)	Pearson's Correlation	
	mean ± sd	mean ± sd	r	p-value		mean ± sd	mean ± sd	r	p-value
450	1.13 ± 0.62	2.05 ± 1.18	0.90	<0.00	**760**	1.92 ± 0.77	1.83 ± 0.74	0.98	<0.00
460	0.48 ± 0.37	1.41 ± 1.10	0.62	<0.00	**770**	1.87 ± 0.75	1.84 ± 0.75	0.98	<0.00
470	0.45 ± 0.38	1.15 ± 0.74	0.49	<0.00	**780**	1.90 ± 0.78	1.86 ± 0.78	0.98	<0.00
480	0.36 ± 0.40	0.90 ± 0.59	0.30	0.02	**790**	1.94 ± 0.79	1.88 ± 0.79	0.98	<0.00
490	0.35 ± 0.41	0.86 ± 0.53	0.29	0.03	**800**	1.96 ± 0.80	1.90 ± 0.77	0.99	<0.00
500	0.33 ± 0.38	0.82 ± 0.46	0.29	0.02	**810**	1.96 ± 0.80	1.90 ± 0.77	0.98	<0.00
510	0.39 ± 0.50	0.83 ± 0.44	0.23	0.08	**820**	1.98 ± 0.80	1.91 ± 0.80	0.98	<0.00
520	0.46 ± 0.59	0.89 ± 0.44	0.20	0.13	**830**	1.88 ± 0.76	1.90 ± 0.78	0.98	<0.00
530	0.56 ± 0.58	0.98 ± 0.46	0.22	0.10	**840**	1.87 ± 0.74	1.87 ± 0.76	0.98	<0.00
540	0.66 ± 0.49	1.10 ± 0.55	0.32	0.01	**850**	1.80 ± 0.73	1.88 ± 0.77	0.99	<0.00
550	0.81 ± 0.46	1.20 ± 0.60	0.38	0.00	**860**	1.79 ± 0.72	1.87 ± 0.74	0.99	<0.00
560	0.88 ± 0.48	1.25 ± 0.67	0.40	0.00	**870**	1.80 ± 0.72	1.87 ± 0.76	0.98	<0.00
570	0.97 ± 0.51	1.31 ± 0.66	0.40	0.00	**880**	1.74 ± 0.70	1.86 ± 0.76	0.98	<0.00
580	1.12 ± 0.50	1.40 ± 0.70	0.53	<0.00	**890**	1.72 ± 0.68	1.84 ± 0.76	0.98	<0.00
590	1.31 ± 0.53	1.52 ± 0.73	0.71	<0.00	**900**	1.67 ± 0.65	1.84 ± 0.75	0.98	<0.00
600	1.53 ± 0.60	1.58 ± 0.71	0.86	<0.00	**910**	1.63 ± 0.65	1.82 ± 0.73	0.98	<0.00
610	1.71 ± 0.70	1.65 ± 0.69	0.93	<0.00	**920**	1.56 ± 0.62	1.80 ± 0.72	0.98	<0.00
620	1.85 ± 0.79	1.73 ± 0.69	0.95	<0.00	**930**	1.49 ± 0.59	1.74 ± 0.68	0.98	<0.00
630	1.93 ± 0.84	1.78 ± 0.71	0.96	<0.00	**940**	1.39 ± 0.55	1.67 ± 0.68	0.98	<0.00
640	1.98 ± 0.86	1.80 ± 0.73	0.96	<0.00	**950**	1.19 ± 0.52	1.60 ± 0.66	0.93	<0.00
650	2.02 ± 0.89	1.85 ± 0.75	0.96	<0.00	**960**	1.17 ± 0.48	1.53 ± 0.67	0.96	<0.00
660	2.04 ± 0.92	1.85 ± 0.77	0.96	<0.00	**970**	1.14 ± 0.47	1.51 ± 0.64	0.95	<0.00
670	2.05 ± 0.95	1.88 ± 0.81	0.96	<0.00	**980**	1.12 ± 0.46	1.52 ± 0.65	0.95	<0.00
680	2.09 ± 0.95	1.91 ± 0.87	0.95	<0.00	**990**	1.14 ± 0.46	1.53 ± 0.70	0.95	<0.00
690	2.02 ± 0.93	1.97 ± 0.81	0.97	<0.00	**1000**	1.15 ± 0.46	1.55 ± 0.68	0.95	<0.00
700	2.12 ± 0.89	1.89 ± 0.79	0.98	<0.00	**1010**	1.18 ± 0.47	1.57 ± 0.66	0.95	<0.00
710	2.09 ± 0.87	1.89 ± 0.78	0.98	<0.00	**1020**	1.22 ± 0.49	1.63 ± 0.71	0.95	<0.00
720	2.04 ± 0.85	1.87 ± 0.82	0.98	<0.00	**1030**	1.28 ± 0.51	1.70 ± 0.76	0.96	<0.00
730	1.96 ± 0.80	1.85 ± 0.78	0.98	<0.00	**1040**	1.35 ± 0.53	1.82 ± 0.78	0.96	<0.00
740	1.88 ± 0.77	1.82 ± 0.76	0.98	<0.00	**1050**	1.42 ± 0.56	2.00 ± 0.85	0.96	<0.00
750	1.87 ± 0.76	1.83 ± 0.77	0.98	<0.00					

λ = wavelength; sd = standard deviation.

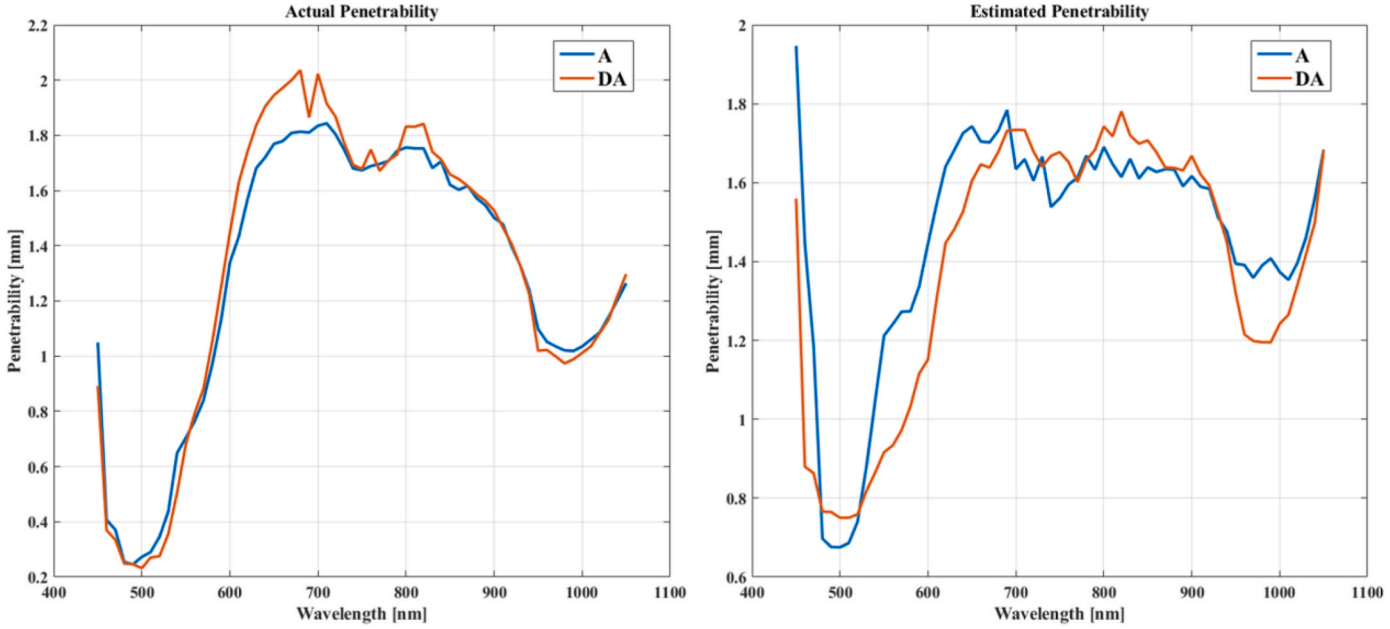

Fig. 5. Comparison between astringent (A) and deastringed (DA) persimmon fruit: averaged actual penetrability depth (left) and averaged estimated penetrability depth (right).

The results of the goodness-of-fit features (R^2, RMSE and RPD) of the linear regression models for each spectral wavelength are shown in Table 2. The wavelengths that presented the high performance ($R^2 > 0.8$ and RPD>2.5) to estimate the light penetrability depth ranged from 610 nm to 1050 nm (Table 2), showing a low performance in the rest. This proves that the estimated light penetration depth is reliable in the range from 610 nm to 1050 nm, although it is not confirmed in the range from 450 nm to 600 nm.

Some linear regressions were plotted in Fig. 6. The close relationship between the actual and estimated depth values above 610 nm shows a strong correlation between the two variables. It can be observed the presence of a sample whose estimated penetrability exceeds the mean

Table 2
Performance criteria of linear regression for each wavelength.

λ (nm)	R^2	RMSE	RPD	λ (nm)	R^2	RMSE	RPD	λ (nm)	R^2	RMSE	RPD
450	0.81	0.52	2.27	**660**	0.92	0.22	3.56	**870**	0.97	0.13	5.63
460	0.36	0.90	1.24	**670**	0.92	0.23	3.44	**880**	0.97	0.14	5.52
470	0.22	0.67	1.13	**680**	0.90	0.27	3.18	**890**	0.96	0.14	5.24
480	0.09	0.57	1.04	**690**	0.93	0.21	3.80	**900**	0.97	0.13	5.63
490	0.08	0.51	1.03	**700**	0.96	0.17	4.73	**910**	0.97	0.13	5.49
500	0.09	0.45	1.04	**710**	0.96	0.16	4.99	**920**	0.97	0.13	5.37
510	0.05	0.43	1.02	**720**	0.96	0.17	4.82	**930**	0.97	0.13	5.32
520	0.04	0.44	1.01	**730**	0.96	0.15	5.26	**940**	0.96	0.14	4.68
530	0.05	0.46	1.02	**740**	0.96	0.15	4.94	**950**	0.86	0.25	2.61
540	0.10	0.53	1.05	**750**	0.96	0.15	5.04	**960**	0.92	0.19	3.46
550	0.15	0.56	1.07	**760**	0.96	0.15	4.83	**970**	0.90	0.20	3.21
560	0.16	0.62	1.08	**770**	0.97	0.14	5.37	**980**	0.90	0.21	3.13
570	0.16	0.61	1.08	**780**	0.97	0.14	5.64	**990**	0.90	0.22	3.19
580	0.28	0.60	1.17	**790**	0.97	0.15	5.38	**1000**	0.91	0.21	3.28
590	0.50	0.52	1.40	**800**	0.97	0.13	5.90	**1010**	0.91	0.20	3.27
600	0.74	0.37	1.94	**810**	0.96	0.15	5.30	**1020**	0.90	0.23	3.11
610	0.86	0.26	2.69	**820**	0.96	0.15	5.25	**1030**	0.92	0.21	3.62
620	0.90	0.22	3.08	**830**	0.97	0.14	5.48	**1040**	0.92	0.22	3.58
630	0.92	0.20	3.60	**840**	0.96	0.16	4.72	**1050**	0.91	0.25	3.38
640	0.93	0.19	3.72	**850**	0.97	0.13	5.88				
650	0.93	0.20	3.64	**860**	0.97	0.13	5.78				

λ = wavelength; RMSE = root mean square error; RPD = ratio of performance to deviation.

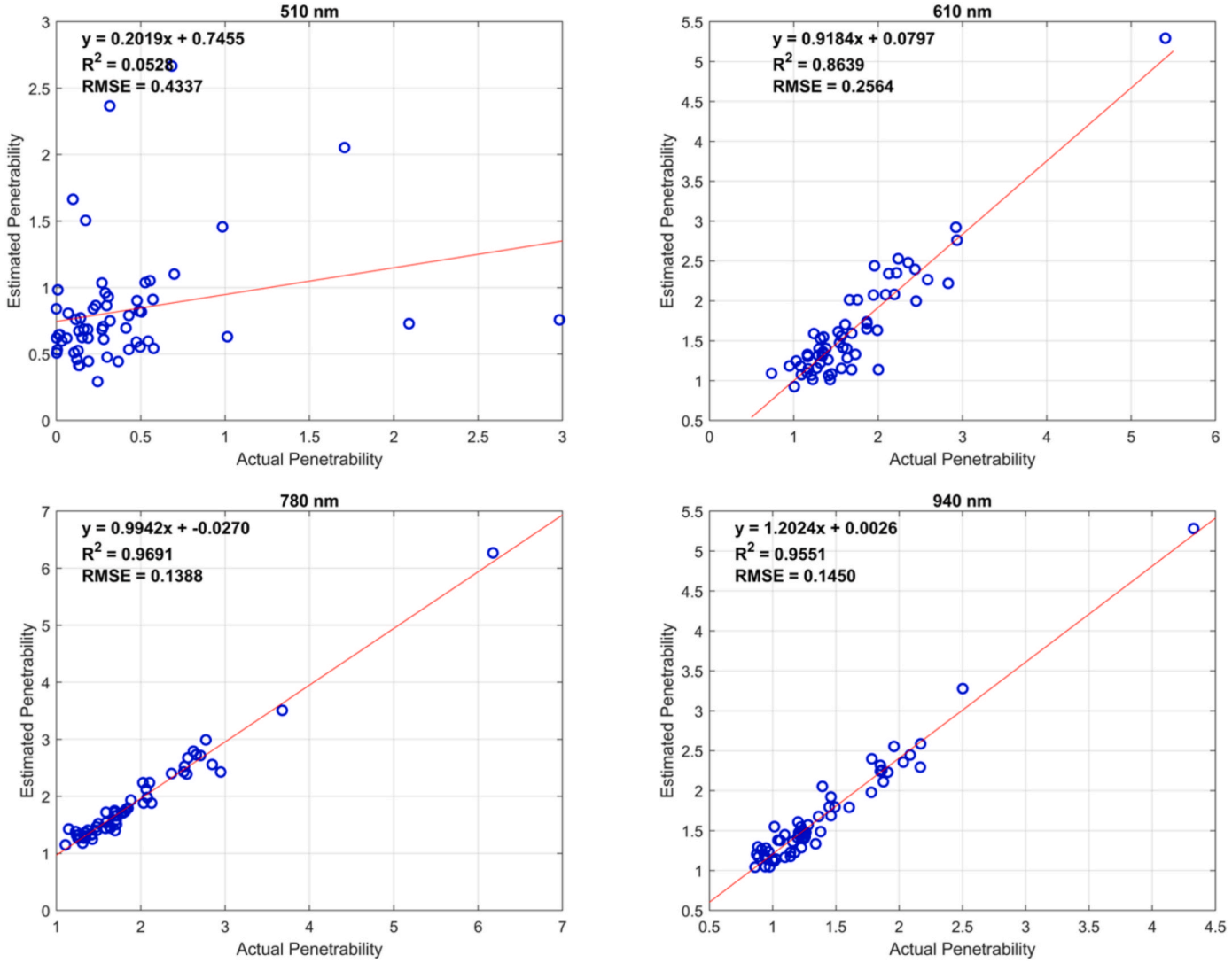

Fig. 6. Estimated by actual penetrability depth value scatter plots for four selected wavelengths (510, 610, 780 and 940 nm).

value, which can be due to the heterogeneous nature of the persimmon samples used in this study. In order to ensure this sample was not an outlier, it was removed from the regression, and similar values of R^2 and RMSE were obtained. In fact, the estimated value of light penetration depth turned out a close value to the actual one, indicating that this sample was valid and, therefore, not removed from the analysis.

Nevertheless, the fact that no relationship was found in this range was expected according to Farrell's diffusion theory. This theory can only be used when the reduced scattering is much higher than absorption ($\mu's \gg \mu_a$) (Martelli et al., 2009). However, this condition is not always fulfilled in biological tissues due to the high absorption coefficient of biological chromophores, as is the case of carotenoids, anthocyanins or chlorophylls, which are dominant in fruit and vegetable tissues and responsible for colour. In addition, it is known that the persimmon spectral reflectance experiences a high absorption in the range of 450–600 nm due to these chromophores (Munera et al., 2019a; Rajkumar et al., 2012). Therefore, this inherent characteristic is responsible for the uncorrelated results obtained in this range, confirming the accuracy of the Vis-NIR HSI-based systems and Farrell's diffusion theory used to estimate the light penetrability depth.

According to Equation (9), the estimated penetrability is related to the values of the absorption and reduced scattering coefficients. This relationship is really useful because the absorption and scattering can be validated indirectly by comparing them to the actual penetrability. Thus, the close relationship between the estimated and actual light penetrability depth values obtained in this study in the wavelengths between 610 nm and 1050 nm reinforces that the non-destructive HSI-based systems can measure absorption and reduce scattering reliably. Therefore, this methodology accurately estimated the penetrability of light on persimmon fruit, where the maximum depth was reached no more than 2 mm.

This result confirms that HSI system in the range 450–1050 nm can only obtain the spectral information of the outermost tissues of the persimmon fruit, being unable to identify certain molecules and compounds distributed within the flesh directly. This is the case of the water-soluble tannins, molecules that are heterogeneously located in the flesh of 'Rojo Brillante' persimmon fruit (Munera et al., 2017). Munera et al. (2019) attempted to estimate non-destructively the content of these molecules in this cultivar of persimmon using the same HSI system in the same spectral range. Still, they could not accurately detect it when the content was low. They concluded that this imaging technology could predict the physiological and structural changes that persimmon fruit undergoes in the outermost tissues during the deastringency process, but not these molecules directly.

There are numerous works in the literature based on spectroscopy and hyperspectral imaging with the aim of evaluating non-destructively the internal quality of fruits with different skin thickness, flesh translucency and size (Arendse et al., 2018; Cortés et al., 2019; Li et al., 2019; Y. Lu et al., 2020; Walsh et al., 2020; Alamar et al., 2023). In either case, the methodology proposed here could provide important information when designing an experiment, selecting a specific spectral and illumination system, offering explanations for variations in the prediction of quality parameters, and understanding the depth of light penetration into the tissue.

Regarding the estimation of light penetration depth in fruit, no works have been found in the literature based on HSI technology, and only a few have been found using spectroscopy. The here estimated light penetrability depth differs from those obtained in previous studies performed destructively in apples and using spectroscopy (Lammertyn et al., 2000; Monago-Maraña et al., 2021), where values from 2 mm to 8 mm were obtained. These differences in penetrability depth were possibly due to the use of one-point spectroscopy systems and different light configurations and also to the difference in the fruit studied.

4. Conclusions

In this study, a non-destructive HSI-based SR approach developed to estimate the depth of light penetration in the fruit using a Vis-NIR region was validated. This validation was performed by comparing the light penetrability depth, which was calculated using the estimated absorption and reduced scattering, with the actual penetrability light depth measured by a destructive study specially designed for this purpose. The results obtained demonstrated that the proposed non-destructive approach is helpful for measuring the absorption and reduced scattering features of persimmon fruit over the spectral range 610–1050 nm. The depth of penetrability obtained by both protocols (estimated and actual) presented a high relationship ($R^2 > 0.8$ and RPD>2.5). However, the penetrability estimated for persimmon fruit was limited to a maximum depth of 2 mm.

This particular study on persimmon fruit has demonstrated that the information is only extracted from the flesh layers closest to the surface because the light only penetrates a few millimetres inside the fruit. This fact confirms HSI systems' challenges in acquiring information on the fruit. This non-destructive approach could be a key method to know the optical properties of any fruit, taking into account the optical and illumination system used and being able to accurately estimate the quality properties of the fruit at a particular and known depth.

In future work, further studies will be carried out to evaluate the penetration depth using a wider range of wavelengths, as the present study was conducted within the range between 450 and 1050 nm. Also, to state that this non-destructive HSI approach is effective, other types of fruit with different skin thicknesses will be tested. Finally, more studies should be done to evaluate the influence of the illumination power and the length of light incidence on the fruit tissues.

Credit author statement

Alejandro Rodríguez-Ortega: Conceptualization, Investigation, Methodology, Formal analysis, Investigation, Writing – original draft. **Nuria Aleixos:** Supervision, Project administration, Writing – review & editing. **José Blasco:** Funding acquisition, Resources, Writing – review & editing. **Francisco Albert:** Software, Data curation. **Sandra Munera:** Writing – review & editing, Visualization.

Declaration of competing interest

The authors declare that they have no known competing financial interests or personal relationships that could have appeared to influence the work reported in this paper.

Data availability

Data will be made available on request.

Acknowledgments

This work was co-funded by the projects AEI PID 2019-107347RR-C31 and PID 2019-107347RR-C32, and GVA-PROMETEO CIPROM/2021/014. Sandra Munera thanks the postdoctoral contract Juan de la Cierva-Formación (FJC2021-047786-I) co-funded by MCIN/AEI/10.13039/501100011033 and NextGenerationEU/PRTR.

References

Alamar, M.C., Aleixos, N., Amigo, J.M., Barbin, D.F., Blasco, J., 2023. Hyperspectral imaging techniques for quality and safety assessment in fresh horticultural produce and prospects for measurement of mechanical damage. In: Pathare, Pankaj B., Opara, Umezuruike Linus (Eds.), Mechanical Damage in Fresh Horticultural Produce - Measurement, Analysis and Control (in press).

Arendse, E., Fawole, O.A., Magwaza, L.S., Opara, U.L., 2018. Non-destructive prediction of internal and external quality attributes of fruit with thick rind: a review. J. Food Eng. 217, 11–23. https://doi.org/10.1016/J.JFOODENG.2017.08.009.

Berndt, K.W., Moulton, J.D., Patterson, M.S., Lakowicz, J.R., Wilson, B.C., 1991. Frequency-domain reflectance for the determination of the scattering and absorption properties of tissue. Appl. Opt. 30 (31), 4474–4476. https://doi.org/10.1364/AO.30.004474, 30, 4474–4476.

Cen, Haiyan, Lu, R., Mendoza, F.A., 2012a. Analysis of absorption and scattering spectra for assessing the internal quality of apple fruit. Acta Hortic. 945, 181–188. https://doi.org/10.17660/ACTAHORTIC.2012.945.24.

Cen, H., Lu, R., Mendoza, F.A., Ariana, D.P., 2012b. Assessing multiple quality attributes of peaches using optical absorption and scattering properties. Transactions of the ASABE 55, 647–657. https://doi.org/10.13031/2013.41366.

Coleman, T.F., Li, Y., 2006. An interior trust region approach for nonlinear minimization. Subject to Bounds 6, 418–445. https://doi.org/10.1137/0806023.

Cortés, V., Blasco, J., Aleixos, N., Cubero, S., Talens, P., 2019. Monitoring strategies for quality control of agricultural products using visible and near-infrared spectroscopy: a review. Trends Food Sci. Technol. 85, 138–148. https://doi.org/10.1016/J.TIFS.2019.01.015.

Cortés, V., Rodríguez, A., Blasco, J., Rey, B., Besada, C., Cubero, S., Salvador, A., Talens, P., Aleixos, N., 2017. Prediction of the level of astringency in persimmon using visible and near-infrared spectroscopy. J. Food Eng. 204, 27–37. https://doi.org/10.1016/J.JFOODENG.2017.02.017.

Das, A.K., Islam, M.N., Faruk, M.O., Ashaduzzaman, M., Dungani, R., 2020. Review on tannins: extraction processes, applications and possibilities. South Afr. J. Bot. 135, 58–70. https://doi.org/10.1016/j.sajb.2020.08.008.

Farrell, T.J., Patterson, M.S., Wilson, B., 1992. A diffusion theory model of spatially resolved, steady-state diffuse reflectance for the noninvasive determination of tissue optical properties in vivo. Med. Phys. 19, 879–888. https://doi.org/10.1118/1.596777.

Geladi, P., MacDougall, D., Martens, H., 1985. Linearization and scatter-correction for near-infrared reflectance spectra of meat. Appl. Spectrosc. 39 (3), 491–500, 39, 491–500.

Giordani, E., Doumett, S., Nin, S., Del Bubba, M., 2011. Selected primary and secondary metabolites in fresh persimmon (*Diospyros kaki* Thunb.): a review of analytical methods and current knowledge of fruit composition and health benefits. Food Res. Int. 44, 1752–1767. https://doi.org/10.1016/j.foodres.2011.01.036.

Hemrattrakun, P., Nakano, K., Boonyakiat, D., Ohashi, S., Maniwara, P., Theanjumpol, P., Seehanam, P., 2021. Comparison of reflectance and interactance modes of visible and near-infrared spectroscopy for predicting persimmon fruit quality. Food Anal. Methods 14, 117–126. https://doi.org/10.1007/S12161-020-01853-W/FIGURES/4.

Hu, D., Fu, X., Wang, A., Ying, Y., 2015. Measurement methods for optical absorption and scattering properties of fruits and vegetables. Transactions of the ASABE 58, 1387–1401. https://doi.org/10.13031/TRANS.58.11103.

Hu, D., Lu, R., Ying, Y., 2018. A two-step parameter optimization algorithm for improving estimation of optical properties using spatial frequency domain imaging. J. Quant. Spectrosc. Radiat. Transf. 207, 32–40. https://doi.org/10.1016/J.JQSRT.2017.12.022.

Kho, E., de Boer, L.L., Post, A.L., Van de Vijver, K.K., Jóźwiak, K., Sterenborg, H.J.C.M., Ruers, T.J.M., 2019. Imaging depth variations in hyperspectral imaging: development of a method to detect tumor up to the required tumor-free margin width. J. Biophot. 12 https://doi.org/10.1002/jbio.201900086.

Kienle, A., Lilge, L., Hibst, R., Patterson, M.S., Wilson, B.C., Steiner, R., 1996. Spatially resolved absolute diffuse reflectance measurements for noninvasive determination of the optical scattering and absorption coefficients of biological tissue. Appl. Opt. 35 (13), 2304–2314. https://doi.org/10.1364/AO.35.002304, 35, 2304–2314.

Lammertyn, J., Peirs, A., De Baerdemaeker, J., Nicolaï, B., 2000. Light penetration properties of NIR radiation in fruit with respect to non-destructive quality assessment. Postharvest Biol. Technol. 18, 121–132. https://doi.org/10.1016/S0925-5214(99)00071-X.

Li, S., Luo, H., Hu, M., Zhang, M., Feng, J., Liu, Y., Dong, Q., Liu, B., 2019. Optical non-destructive techniques for small berry fruits: a review. Artif. Intell. Agri. 2, 85–98. https://doi.org/10.1016/J.AIIA.2019.07.002.

Lorente, D., Zude, M., Idler, C., Gómez-Sanchis, J., Blasco, J., 2015. Laser-light backscattering imaging for early decay detection in citrus fruit using both a statistical and a physical model. J. Food Eng. 154, 76–85. https://doi.org/10.1016/J.JFOODENG.2015.01.004.

Lorente, D., Zude, M., Regen, C., Palou, L., Gómez-Sanchis, J., Blasco, J., 2013. Early decay detection in citrus fruit using laser-light backscattering imaging. Postharvest Biol. Technol. 86, 424–430. https://doi.org/10.1016/J.POSTHARVBIO.2013.07.021.

Lu, R., Van Beers, R., Saeys, W., Li, C., Cen, H., 2020. Measurement of optical properties of fruits and vegetables: a review. Postharvest Biol. Technol. 159, 111003 https://doi.org/10.1016/j.postharvbio.2019.111003.

Lu, Y., Huang, Y., Lu, R., 2017. Innovative hyperspectral imaging-based techniques for quality evaluation of fruits and vegetables: a review, 2017 Appl. Sci. 7. https://doi.org/10.3390/APP7020189. Page 189 7, 189.

Lu, Y., Saeys, W., Kim, M., Peng, Y., Lu, R., 2020. Hyperspectral imaging technology for quality and safety evaluation of horticultural products: a review and celebration of the past 20-year progress. Postharvest Biol. Technol. 170, 111318 https://doi.org/10.1016/J.POSTHARVBIO.2020.111318.

Ma, T., Zhao, J., Inagaki, T., Su, Y., Tsuchikawa, S., 2022. Rapid and nondestructive prediction of firmness, soluble solids content, and pH in kiwifruit using Vis–NIR spatially resolved spectroscopy. Postharvest Biol. Technol. 186, 111841 https://doi.org/10.1016/J.POSTHARVBIO.2022.111841.

Martelli, F., Del Bianco, S., Ismaelli, A., Zaccanti, G., 2009. Light propagation through biological tissue and other diffusive media: theory, solutions, and software. Light Propagation Through Biological Tissue and Other Diffusive Media: Theor. Solut. 1–275. https://doi.org/10.1117/3.824746 and Software.

Monago-Maraña, O., Afseth, N.K., Knutsen, S.H., Wubshet, S.G., Wold, J.P., 2021. Quantification of soluble solids and individual sugars in apples by Raman spectroscopy: a feasibility study. Postharvest Biol. Technol. 180, 111620 https://doi.org/10.1016/J.POSTHARVBIO.2021.111620.

Munera, S., Aleixos, N., Besada, C., Gómez-Sanchis, J., Salvador, A., Cubero, S., Talens, P., Blasco, J., 2019. Discrimination of Astringent and Deastringed Hard "Rojo Brillante" Persimmon Fruit Using a Sensory Threshold by Means of Hyperspectral Imaging. https://doi.org/10.1016/j.jfoodeng.2019.06.008.

Munera, S., Besada, C., Aleixos, N., Talens, P., Salvador, A., Sun, D.W., Cubero, S., Blasco, J., 2017. Non-destructive assessment of the internal quality of intact persimmon using colour and VIS/NIR hyperspectral imaging. Lebensm. Wiss. Technol. 77, 241–248. https://doi.org/10.1016/J.LWT.2016.11.063.

Munera, S., Rodríguez-Ortega, A., Aleixos, N., Cubero, S., Gómez-Sanchis, J., Blasco, J., 2021. Detection of invisible damages in 'rojo Brillante' persimmon fruit at different stages using hyperspectral imaging and chemometrics. Foods 10, 2170. https://doi.org/10.3390/foods10092170.

Pedrotti, F.L., Pedrotti, L.M., Pedrotti, L.S., 2007. In: Introduction to Optics, third ed. Cambridge University Press. 978-1-108-42826-2.

Qin, J., Lu, R., 2008. Measurement of the optical properties of fruits and vegetables using spatially resolved hyperspectral diffuse reflectance imaging technique. Postharvest Biol. Technol. 49, 355–365. https://doi.org/10.1016/J.POSTHARVBIO.2008.03.010.

Rajkumar, P., Wang, N., Eimasry, G., Raghavan, G.S.V., Gariepy, Y., 2012. Studies on banana fruit quality and maturity stages using hyperspectral imaging. J. Food Eng. 108, 194–200. https://doi.org/10.1016/J.JFOODENG.2011.05.002.

Rodrigues, E.M., Hemmer, E., 2022. Trends in hyperspectral imaging: from environmental and health sensing to structure-property and nano-bio interaction studies. Anal. Bioanal. Chem. https://doi.org/10.1007/S00216-022-03959-Y, 2022 1–11.

Saeys, W., Velazco-Roa, M.A., Thennadil, S.N., Ramon, H., Nicolaï, B.M., 2008. Optical properties of apple skin and flesh in the wavelength range from 350 to 2200 nm. Appl. Opt. 47 (7), 908–919 47. https://doi.org/10.1364/AO.47.000908, 908–919.

Salvador, A., Arnal, L., Besada, C., Larrea, V., Quiles, A., Pérez-Munuera, I., 2007. Physiological and structural changes during ripening and deastringency treatment of persimmon fruit cv. 'Rojo Brillante.' Postharvest Biol. Technol. 46, 181–188. https://doi.org/10.1016/J.POSTHARVBIO.2007.05.003.

Si, W., Xiong, J., Huang, Y., Jiang, X., Hu, D., 2022. Quality assessment of fruits and vegetables based on spatially resolved spectroscopy: a review. Foods 11. https://doi.org/10.3390/FOODS11091198.

Sun, Y., Huang, Y., Pan, L., Wang, X., 2021. Evaluation of the changes in optical properties of peaches with different maturity levels during bruising. Foods 10. https://doi.org/10.3390/foods10020388.

Tian, S., Xu, H., 2022. Mechanical-based and optical-based methods for nondestructive evaluation of fruit firmness. Food Rev. Int. https://doi.org/10.1080/87559129.2021.2015376.

Van Beers, R., Aernouts, B., León Gutiérrez, L., Erkinbaev, C., Rutten, K., Schenk, A., Nicolaï, B., Saeys, W., 2015. Optimal illumination-detection distance and detector size for predicting braeburn apple maturity from Vis/NIR laser reflectance measurements. Food Bioprocess Technol. 8, 2123–2136. https://doi.org/10.1007/S11947-015-1562-4/FIGURES/8.

Vanoli, M., Van Beers, R., Sadar, N., Rizzolo, A., Buccheri, M., Grassi, M., Lovati, F., Nicolaï, B., Aernouts, B., Watté, R., Torricelli, A., Spinelli, L., Saeys, W., Zanella, A., 2020. Time- and spatially-resolved spectroscopy to determine the bulk optical properties of 'Braeburn' apples after ripening in shelf life. Postharvest Biol. Technol. 168, 111233 https://doi.org/10.1016/J.POSTHARVBIO.2020.111233.

Walsh, K.B., Blasco, J., Zude-Sasse, M., Sun, X., 2020. Visible-NIR 'point' spectroscopy in postharvest fruit and vegetable assessment: the science behind three decades of commercial use. Postharvest Biol. Technol. 168, 111246 https://doi.org/10.1016/J.POSTHARVBIO.2020.111246.

Wang, Z., Van Beers, R., Aernouts, B., Watté, R., Verboven, P., Nicolaï, B., Saeys, W., 2020. Microstructure affects light scattering in apples. Postharvest Biol. Technol. 159, 110996 https://doi.org/10.1016/J.POSTHARVBIO.2019.110996.

Welch, A.J., van Gemert, M.J., Star, W.M., 2010. Definitions and overview of tissue optics. In: Welch, A., van Gemert, M. (Eds.), Optical-Thermal Response of Laser-Irradiated Tissue. Springer, Dordrecht. https://doi.org/10.1007/978-90-481-8831-4_3.

Wilson, B.C., Chance, B., Patterson, M.S., 1989. Time resolved reflectance and transmittance for the noninvasive measurement of tissue optical properties. Appl. Opt. 28 (12), 2331–2336. https://doi.org/10.1364/AO.28.002331, 28, 2331–2336.

Wilson, B.C., Jacques, S.L., 1990. Optical reflectance and transmittance of tissues: principles and applications. IEEE J. Quant. Electron. 26, 2186–2199. https://doi.org/10.1109/3.64355.

Xuan, G., Gao, C., Shao, Y., 2022. Spectral and image analysis of hyperspectral data for internal and external quality assessment of peach fruit. Spectrochim. Acta Mol. Biomol. Spectrosc. 272, 121016 https://doi.org/10.1016/J.SAA.2022.121016.

Ying, Y., Xie, L., Fu, X., 2016. Spectral scattering for assessing the quality of fruits and vegetables. In: Lu, Renfu (Ed.), Light Scattering Technology for Food Property, Quality and Safety Assessment. CRC Press, Taylor & Francis Group, Boca Raton, FL, pp. 225–250, 33487-2742, ISBN: 978-1-4822-6334-3.

Zhu, Q., He, C., Lu, R., Mendoza, F., Cen, H., 2015. Ripeness evaluation of 'Sun Bright' tomato using optical absorption and scattering properties. Postharvest Biol. Technol. 103, 27–34. https://doi.org/10.1016/J.POSTHARVBIO.2015.02.007.